Mesoporous gold electrodes for sensors based on electrochemical double layer capacitance

Alessia Mortari[‡§], Abbas Maaroof[‡], Donald Martin[‡] and Michael B. Cortie[‡*]

[‡]Institute for Nanoscale Technology, University of Technology Sydney, Australia

[§]On leave from the Department of Analytical Chemistry, Lund University, Sweden

ABSTRACT

The use of mesoporous gold as electrode material for measurement of electrochemical capacitance is investigated. The electrodes possess a pore size in the range of 10 to 30 nm and are prepared by de-alloying films of $AuAl_x$, where $x \geq 2$. Analyses conducted with X-ray photoelectron spectra (XPS) show that their surfaces are essentially pure gold, with only traces of aluminium remaining. The electrodes show near-ideal capacitor behaviour under both cyclic voltammetry and potential-step conditions. The higher capacitance of the mesoporous electrodes leads to a better dynamic range in potential-step experiments, resulting in improved accuracy of measurement. The sensitivity of the new material as a capacitive sensor is demonstrated in a milk fouling experiment, and is improved by up to 30 times compared to the control sample of ordinary planar gold. We propose that the use of mesoporous gold electrodes offer a convenient way to sensitively and accurately amplify the capacitance signal of an electrochemical sensor.

KEYWORDS: double layer capacitance, capacitive sensor, mesoporous gold, nanoporous gold, accuracy, sensitivity.

---

* Institute for Nanoscale Technology, University of Technology Sydney,

PO Box 123, Broadway, NSW 2007, Australia; ph. +61-2-9514-2208; fax +61-2-9514-7553; e-mail: michael.cortie@uts.edu.au

1. Introduction

Electrochemical capacitive sensors have been proposed or used for many different applications [1, 2] and can serve as a transducting platform on which to design diverse biosensors [3]. In general, emphasis in this field has been placed on developing new signal processing systems [4, 5] and sensor interfaces [4, 6, 7] in order to increase the accuracy of capacitance measurement. Nearly all of the existing applications are based on planar or cylindrical metallic electrodes. However, porous or mesoporous metallic structures can also be envisaged for electrodes. Porous metallic surfaces produced by electrodeposition , de-alloying or colloidal aggregation have interesting new properties [8-10] and have found practical or potential applications as electrodes in electrochemical devices such as super-capacitors [11, 12] and as sensor substrates for optical techniques such as surface enhanced Raman spectroscopy (SERS) or surface plasmon spectroscopy, e.g. [13, 14]. Mesoporous metal electrodes produced by de-alloying can have particularly high specific surface areas, in excess of 2 m^2/g, and possess tortuous and semi-enclosed pores. The high surface area leads directly to an enhanced electrochemical double layer capacitance, since the capacitance, C, is proportional to the surface area, S, via the standard relationship:

$$C = \frac{\varepsilon \varepsilon_0 S}{d} \qquad (1)$$

where ε is the dielectric constant of the medium, ε_0 is the permeability of free space and d the inter-plate distance. In the present instance d can be taken as the thickness of the electrical double layer developed around the electrodes.

Compared to a planar gold electrode of same nominal area, mesoporous gold (also known as Raney gold [8, 15], or nanoporous gold [16]) has a significantly increased specific surface area and therefore electrolytic capacitance [12]. Like planar gold it can be readily produced in thin films [17] but its advantage in respect of capacitance appears not to have been exploited yet in sensor design. Here we propose that the use of this material in electrodes could lead to the development of capacitive sensors of improved sensitivity and accuracy. To address this hypothesis, two different kinds of mesoporous gold were developed and compared to each other and to conventional sputtered gold electrodes. The microstructure, chemical composition and electrochemical stability of the gold coatings was characterized, while the electrochemical double-layer

formation was studied using cyclic voltammetry. The capacitance values were independently determined using potential step experiments, and cyclic voltammetry. Finally, to verify the sensitivity of the experimental electrodes, the proteinaceous fouling that occurs on surfaces immersed in milk was used as a dynamic test.

2. Experimental materials and methods

2.1 Preparation of mesoporous metal films

Mesoporous gold films were made by de-alloying thin films comprised either of the intermetallic compound $AuAl_2$, or very fine-scale mixtures of it with Al. The starting films were prepared by co-depositing the elements using high vacuum direct current magnetron sputtering, applied onto glass microscope slides through a 15 x 15 mm hole in a thin mica mask. The sputtering targets of Au and Al were 99.999% pure discs (50 mm diameter) placed 150 mm away from the substrate. The base pressure was better than ~$1x10^{-4}$ Pa (~10^{-6} torr) while sputtering was carried out in the presence of flowing Ar at a pressure of 0.25 Pa ($2x10^{-3}$ torr) with a 3kV 10W radio frequency (RF) biased substrate. To ensure good homogeneity and crystallinity, the substrate was heated to 400°C during deposition. The aluminum was subsequently removed from the compound by immersing the films in 0.2 M aqueous NaOH solution for about one minute.

Three types of sample are discussed in this paper. They are designated '*100mesoAu*', consisting of a mesoporous layer of Au that is nominally 100 nm thick and deposited as $AuAl_2$, '*5050mesoAu*', a coating consisting of 50 nm of solid gold on top of which was 50 nm of mesoporous gold deposited as 1Au:4Al (i.e. Al-rich), and '*sAu*', the comparator sample, which consisted of 100 nm of solid gold.

The electrodes were stored under high purity water in order to minimize surface oxidation and non-specific adsorption of particles such as dust, which we found would otherwise inactivate and/or passivate the metal. The electrodes were used within two days of de-alloying.

The In-Lens imaging mode of a Zeiss Supra 55VP scanning electron microscope was used to study the morphology and cross sections of the films. The particular samples studied in this instrument were deposited

onto a silicon substrate (rather than onto glass) in order to ensure that they were electrically grounded in the microscope. The XPS data shown were obtained using Al k_α radiation.

2.2 Capacitance measurement

The electrochemical double layer capacitance developed on the electrodes was measured by two instruments, a cyclic voltammeter, and a custom-built apparatus that applied a potential step to the electrode.

The cyclic voltammetric measurements were performed on an eDAQ potentiostat, using platinum foil as auxiliary electrode, Ag/AgCl as reference electrode and one of the gold samples under investigation as working electrode. Capacitance was calculated from current-potential plots by applying the relation:

$$i = vC \tag{2}$$

where i is the current, v the scan rate and C the capacitance. The cyclic voltammetry experiments were executed under diffusion control.

The custom-built apparatus applied a square wave potential to the electrodes using a constant voltage power supply switched through a reed relay driven by a programmable voltage source (Figure 1). The applied square wave potential cycled between 60 mV for 3 seconds followed by 3 seconds at 0 mV. The voltage transients in the test cell were monitored using a LabJack U12 (LabJack Corporation, www.labjack.com) analogue-to-digital converter interfaced to a computer at an 8 kHz data acquisition rate. A counter-electrode of Pt foil was used. Capacitance was extracted from the data using custom-written software, which exploited the *RC*-induced decay characteristics of the circuit through the expression:

$$V_t = V_0^{\frac{-t}{RC}} \tag{3}$$

where V_t is the recorded discharging potential at time t, V_0 is the applied potential and R is the resistance of the circuit (a 8.2 kΩ resistor was used as an external resistance). The software extracted all data with transient voltages in a user-defined input window (for example, between 60 and 45 mV) and the capacitance was obtained over this range by applying regression on equation 3. Data sets were highly reproducible and produced well-defined semi-logarithmic linear plots of *ln(E) vs t* (see Results and Discussion).

2.3 Electrolytes and test solutions

Potassium phosphate monobasic (H_2KPO_4, Product no. 60220), sodium phosphate dibasic dihydrate ($HNa_2PO_4 \cdot 2H_2O$, Product no. 71644) and potassium chlorate (KCl, Product no. P-3911) were used as-purchased from Sigma-Aldrich to constitute a Phosphate Buffered Saline (PBS) containing $5 \cdot 10^{-3}$ M phosphate buffer pH 7.5 and 0.1 M KCl. All the reagents were of analytical grade and solutions were, if not otherwise specified, prepared using analytical-grade water, produced using a Milli-Q Plus Millipore Water System (Millipore Australia Pty Ltd). Fresh, pasteurized milk was purchased from a convenience store.

3. Results and discussion

3.1 Microstructure and composition of coatings

The surface of both types of mesoporous coating was characterized by fine pores (Figures 2a and 2b) and it was also clear that the surface of the *5050mesoAu* sample was considerably more uneven than that of the *100mesoAu* sample. This effect was common to Al-rich samples and is a consequence of the greater volume of material removed in those cases by de-alloying. The pores in the *100mesoAu* samples were roughly circular in cross section, with openings varying between about 10 and 30 nm in diameter. This is in congruence with pore sizes obtained in previous work [12, 17]. However, those of the *5050mesoAu* sample, while consistently about 10 nm across at their narrowest, were elongated and vermicular (worm-like) in nature. XPS analyses of the surfaces confirmed that they were of elemental Au, with some indications of Al and C contamination (Figure 3).

3.2 Stability study

Non-specific adsorption of particles such as dust and surface oxidation could inactivate and/or passivate metal surfaces. Therefore the capacitance of the three electrode types was also investigated as a function of time (Figure 4). All three samples showed a considerable loss of capacitance over the course of several days. Consequently, in order to minimize the inactivation processes, the electrodes were stored under high purity water and used within three days.

3.3 Cyclic voltammetry and electrochemical double layer formation

The cyclic voltammetry experiments were performed with the purpose of investigating and comparing formation, development and detection of the electrical double layer on the samples *100mesoAu*, *5050mesoA*u and the control sample *sAu*. The gold electrodes were immersed in PBS and cycled in the potential window of interest from 300 to 100 mV and at different scan rates, from 2 to 100 mV/sec. It was necessary to reduce the potential window since the thin mesoporous gold layer peeled off the glass support if held at potentials higher then 500 mV. The potential window was first scanned five times to ensure removal of bubbles and homogeneous diffusion of the buffer ions through the three-dimensional structure to the surface of the gold electrodes. The results presented correspond to the fifth cycle of every measurement. The voltammograms recorded with *100mesoAu* (Figure 5a) exhibited a rectangular shape, especially at slow sweep-rate. This is the characteristic of an ideal capacitor and indicates an unopposed electrolyte motion in the pores. In voltammograms of near-rectangular shape the steepness of the charging process at the switching potential is small. The steepness is generally defined by the capacitance time constant and the equivalent series resistance (ESR), where ESR is formed by the contributions of electrode resistance, bulk electrolyte resistance and the electrolyte resistance in pores. It is reported that small time constants and low resistances are typical of mesoporous structures of conducting materials such as carbon [18, 19]. The voltammogram profiles gradually tilted with the increase of the scan rate, which indicates an increased ohmic resistance of the electrolyte in the pores during fast processes. The same behaviour was observed with *5050mesoAu* (Figure 5b); however, the current developed during the charging and discharging processes was smaller. In contrast, the voltammograms for *sAu* exhibited a depressed shape, and the profile was distorted at the slowest sweep rate (Figure 5c). In this case, the high time constant was mainly due to the resistance of the thin gold layer, which leads to the loss of capacitance at slow scan rates.

The relation between capacitance and scan rate provides an interesting insight into the behaviour of the materials (Figure 6). The sample *sAu* showed little influence of scan rate on the capacitance (rates from 10 to 100 mV/sec) and the capacitance was estimated to be about $1 \cdot 10^{-4}$ F/cm^2. Samples *100mesoAu* and *5050mesoAu* showed two different behaviours in the resulting charging and discharging curves: a first part where the capacitance increased with the scan rate and a second part where the capacitance hardly changed with the increase of scan rate. In the second part of the curves, which corresponds approximately to the *sAu*

scan rate window, the same tendency as *sAu* was displayed and a stable relation between capacitance and sweep rate was observed. The capacitance values in those cases were calculated to be about $1.3 \cdot 10^{-3}$ F/cm^2 and $1.1 \cdot 10^{-3}$ F/cm^2 for *100mesoAu* and *5050mesoAu* respectively (the surface area corresponds to the planar surface area of the electrodes). Those capacitance values are an order of magnitude greater than the ordinary gold *sAu* sample. On the other hand, in the first part of the *100mesoAu* and *5050mesoAu* curves, from 2 to 10 mV/sec, the capacitance increased with the increase of sweep rate. Consequentially there must be an additional or increased limiting factor contributing to the decrease of capacitance at slow scan rates. Ion diffusion in pores is favoured at slow scan rate, while the resistance of the electrode is an intrinsic characteristic of the material and is unaffected by scan rate. At the same time, the diffusion of bulk ions should be constant at the experimental concentration (0.1 M KCl supporting electrolyte in 5 mM phosphate buffer pH 7.5). To verify the effect of the bulk ions diffusion an experiment was run with 10 times higher electrolyte concentration. Under these experimental conditions, the capacitance increased at slow scan rates (results not shown). Consequentially it was deduced that a low ionic concentration was the factor limiting the development of capacitance at the slower scan rates of Figure 6. It is likely that the phenomenon is exacerbated by the impressive increase of real surface within the three dimensional spongy structure of the mesoporous electrodes.

It should be also noted that the charging and discharging processes showed different capacitance values. The disparities may be due to the different diffusion coefficients of the buffer cations and anions. Evidently, use of *100mesoAu* and *5050mesoAu* electrodes allowed a more appreciable distinction between the contributions of the diffusion coefficients than the for the *sAu* electrode.

3.4 Capacitance from square-wave potential steps

Typical results of square-wave potential step experiments in 5 mM PBS buffer pH 7.5, containing 0.1 M KCl supporting electrolyte, are shown in Figure 7a. The interval to completely discharge the *100mesoA*u electrode was greater than the period required to discharge the *5050mesoAu*, which in turn was longer than for the *sAu*. Moreover, the mesoporous samples had the tendency to discharge linearly with time. This behaviour arises from the greater capacitance of the mesoporous materials and linear discharge curves indicate good capacitive behaviour [20].

If the system followed equation 2 exactly there should be a linear relationship between *ln(E)* and *t* in a discharging experiment. However, this is known to be not strictly true for this type of capacitor [21]. In fact, a semi-logarithmic plot of the discharging experiment (Figure 7b) showed that *sAu* presents linearity only in the very first part of the potential decay. Under such conditions, the capacitance extrapolation is obtained from a very limited part of the curve, resulting in poor precision of the measurement [17]. This limitation was overcome by using the mesoporous samples *5050mesoAu* and *100mesoAu* (Table 1). The longer discharge time of the mesoporous electrodes extended the range where linearity between *ln(E)* and *t* exists, increasing dramatically the number of available data points within the capacitance extrapolation range. Specifically, the linear ranges for *5050mesoAu* and *100mesoAu* were 10 and 15 times longer in time than that of the *sAu* sample. The precision of the capacitance detection was then improved accordingly. This difference in discharge characteristics offers the potential for more precise capacitance measurement if mesoporous electrodes are used.

3.5 Fouling in milk

'Fouling' is a well-known process in the dairy industry. Fouling occurs due to milk residues, such as serum proteins, calcium phosphates, casein micelles, fat globules and bacteria that are deposited and remain on the surface of equipment [22]. It is characterized by an initial fast adsorption of milk serum proteins and a subsequent much slower deposition of the other materials. Fouling is an inconvenience for the dairy industry due to loss of milk and the need to ensure thorough cleaning and disinfection of all surfaces exposed to it [22]. Although these deposits can be removed by periodically applied chemical treatments, a more satisfactory solution to the problem would be to also incorporate a means to monitor the build up of the film and a means to validate that it has been removed. In this respect surface electrical properties represent one of the sensing techniques currently in use to monitor fouling and cleaning following its subsequent removal [23].

The electrodes *sAu*, *5050mesoAu* and *100mesoAu* were tested as capacitive sensors for foulant formation. A layer of foulant on an electrode can be schematized as the correspondent equivalent circuit *RC* (Figure 8a) where the total capacitance C_{TOT} is formed from a series of capacitors (Figure 8b) representing essentially the foulant and the double layer of charges (Figure 8c).

The electrodes were placed in fresh, pasteurized milk and a sequence of capacitance measurements initiated using the potential step technique. The results are shown in Figure 9a and in Figure 9b, where the experimental values are normalized based on the starting capacitance level C_0 simply to illustrate the decrease in capacitance for all the electrodes. Each of the electrodes was able to detect the onset of foulant formation and the initial fast adsorption of proteins could be clearly distinguished from the following slow deposition of fats and other materials. However, the sensitivity of the electrodes, calculated as $\Delta C/\Delta t$ during the initial protein adsorption, was impressively different: *sAu* had the lowest sensitivity ($6.89 \cdot 10^{-8}$ F/cm^{2}sec), *5050mesoAu* improved the parameter of 6 times ($4.10 \cdot 10^{-7}$ F/cm^{2}sec) and *100mesoAu* showed the highest sensitivity ($2.00 \cdot 10^{-6}$ F/cm^{2}sec), which was about 30 times greater than the *sAu* performance and about 5 times the *5050mesoAu*. The improvement was probably due to the increased surface of the mesoporous gold electrodes, and it led to a more sensitive capacitance transduction. This enhancement could be generally exploited in sensors and biosensors that measure double layer capacitance.

4. Conclusions

We have shown here that mesoporous gold electrodes have near-ideal capacitor behaviour under both potential-sweep and potential-step conditions. The potential step experiments proved that they can provide a more linear and longer lasting transductance of electrochemical double layer capacitance than ordinary gold surfaces, leading to higher accuracy of measurement. The higher capacitance of the mesoporous electrodes led to a better dynamic range in the measurement signal and improved the sensitivity of the transducer, as confirmed with the tests that followed fouling in milk. Overall, use of mesoporous gold as platform material for electrodes should provide improved performance of capacitive sensor and biosensors within potential step perturbation.

Acknowledgments

The authors thank Ass. Prof. Elisabeth Csöregi from the Department of Analytical Chemistry, Lund University, Sweden, for supporting this project and permitting this collaboration.

References

[1] L. K. Baxter, Capacitive Sensors Design and Applications, IEEE Press, New York, 1997.

[2] S. Baglio, Bio-geochemically inspired capacitive sensors for heavy metals pollution monitoring, IEEE Transactions on Instrumentation and Measurement 52 (2003) 1474-1481.

[3] C. Berggren, B. Bjarnason, G. Johansson, Capacitive biosensors, Electroanalysis 13 (2001) 173-180.

[4] C. Berggren, B. Bjarnason, G. Johansson, Instrumentation for direct capacitive biosensors, Instrumentation Science & Technology 27 (1999) 131-140.

[5] A. S. Hou, S. X.-P. Su, Design of a capacitive-sensor signal processing system with high accuracy and short conversion time, Sensors and Actuators A (2005) 113-119.

[6] A. Burstein, W. J. Kaiser, Mixed analog-digital highly sensitive sensor interface circuit for low-cost microsensors, Sensors and Actuators A (1996) 193-197.

[7] W. Brake, P. Merken, R. Puers, C. V. Hoof, Design methods and algorithms for configurable capacitive sensor interface, Sensors and Actuators A (2005) 25-33.

[8] R. Jurczakowski, C. Hitz, A. Lasia, Impedance of porous Au based electrodes, Journal of Electroanalytical Chemistry 572 (2004) 355–366.

[9] P. Forrer, F. Schlottig, H. Siegenthaler, M. Textor, Electrochemical preparation and surface properties of gold nanowire arrays formed by the template technique, Journal of Applied Electrochemistry 30 (2000) 533-541.

[10] P. N. Bartlett, J. R. Owen, G. S. Attard, J. Elliott, Method of electrodepositing a porous film, United States Patent 6,503,382, 2003.

[11] B. E. Conway, V. Birss, J. Wojtowicz, J. Power Sources 66 (1997) 1-14.

[12] M. B. Cortie, A. I. Maaroof, G. B. Smith, Electrochemical capacitance of mesoporous gold, Gold Bull. 38 (2005) 15-23.

[13] M. J. Natan, B. E. Baker, Self-assembled metal colloid monolayers having size and density gradients, United States Patent 6,242,264, T. P. S. R. Foundation, 2001.

[14] Y. Yang, L. Xiong, J. Shi, M. Nogami, Aligned silver nanorod arrays for surface-enhanced Raman scattering, Nanotechnology 17 (2006) 2670–2674.

[15] J. P. Candy, P. Fouilloux, M. Keddam, H. Takenouti, The characterization of porous electrodes by impedance measurements, Electrochimica Acta 26 (1981) 1029-1034.

[16] J. Erlebacher, M. J. Aziz, A. Karma, N. Dimitrov, K. Sieradzki, Evolution of nanoporosity in dealloying, Nature 410 (2001) 450-435.

[17] M. B. Cortie, A. Maaroof, G. B. Smith, P. Ngoepe, Nanoscale coatings of $AuAl_x$ and $PtAl_x$ and their mesoporous elemental derivatives, Current Applied Physics 6 (2006) 440-443.

[18] J. Lee, S. Yoon, S. M. Oh, C.-H. Shin, T. Hyeon, Development of a new mesoporous carbon using an HMS aluminosilicate template, Adv. Mater. 12 (2000) 359-362.

[19] H.-Y. Liu, K.-P. Wang, H. Teng, A simplified preparation of mesoporous carbon and the examination of the carbon accessibility for electric double layer formation, Carbon 43 (2005) 559-566.

[20] W. Xing, F. Li, Z.-F. Yan, G. Q. Lu, Synthesis and electrochemical properties of mesoporous nickel oxide, J. Power Sources 134 (2004) 324-330.

[21] C. Berggren, B. Bjarnason, G. Johansson, An immunological interleukine-6 capacitive biosensor using perturbation with a potentiostatic step, Biosensors & Bioelectronics 13 (1998) 1061-1068.

[22] P. Walstra, Dairy Technology: Principles of Milk Properties and Processes, Marcel Dekker Incorporated, New York, USA, 1999.

[23] D. I. Wilson, in: P. Watkinson, H. Müller-Steinhagen, and M. R. Malayeri, (Eds.) ECI Conference on Heat Exchanger Fouling and Cleaning: Fundamentals and Applications, Vol. RP1, Article 21, The Berkeley Electronic Press, Santa Fe, New Mexico, USA, 2003, p. 146-157.

FIGURE CAPTIONS

Figure 1. A schematic representation of the apparatus used to determine system capacitance of a test cell.

Figure 2. SEM images of mesoporous gold coatings; (a) *100mesoAu* and (b) *5050mesoAu*.

Figure 3. X-ray photoelectron spectra of mesoporous gold surfaces; (a) *100mesoAu* and (b) *5050mesoAu*.

Figure 4. Electrochemical stability in time of *100mesoAu, 5050mesoAu and sAu electrodes*. The capacitance values were obtained from cyclic voltammetry experiments in 5 mM phosphate buffer pH 7.5 containing 0.1 M KCl, where the potential was scanned from 200 mV to 0 mV at 200 mV/sec scan rate. Capacitance was sampled at 100 mV during the discharging process of the twentieth cycle.

Figure 5. Cyclic voltammograms for (a) *100mesoAu*, (b) *5050mesoAu* and (c) *sAu* electrodes in 5 mM phosphate buffer pH 7.5 containing 0.1 M KCl.

Figure 6. Variation in capacitance of the electrodes as a function of scan rate. Values recorded in 5 mM phosphate buffer pH 7.5 containing 0.1 M KCl.

Figure 7. Discharge of the normal and mesoporous gold electrodes (a) linear in time and (b) plotted against the natural logarithm of time. Values recorded in 5 mM phosphate buffer pH 7.5 containing 0.1 M KCl.

Figure 8. Model for evaluation of potential discharge *vs* time: (a) *RC* circuit where *R* is the dynamic resistance of the foulant layer and C_{TOT} is the capacitance measured between the electrode and the electrolyte solution, (b) the contribution of the capacitance due to the foulant C_f and the double layer of charges C_{dl}, which are schematically drawn in (c).

Figure 9. Fouling of gold surfaces when immersed in pasteurized milk, at room temperature; (a) raw data and (b) normalized comparison of the data sets, where C_0 was the capacitance at time = 0 seconds.

Table 1. Capacitance values and related error, together with number of data points and correlation coefficient, in the linear range from where the capacitance values were obtained (60-45 mV), for the gold electrodes in a square-wave potential step experiments in 5 mM phosphate buffer pH 7.5, containing 0.1 M KCl.

	Capacitance (F/cm^2)	Error (F/cm^2)	Number of data points	Correlation coefficient
sAu	$5.26 \cdot 10^{-5}$	$1.94 \cdot 10^{-6}$	65	0.98
5050mesoAu	$5.80 \cdot 10^{-4}$	$6.47 \cdot 10^{-6}$	650	0.99
100mesoAu	$8.86 \cdot 10^{-4}$	$9.18 \cdot 10^{-6}$	1000	0.99

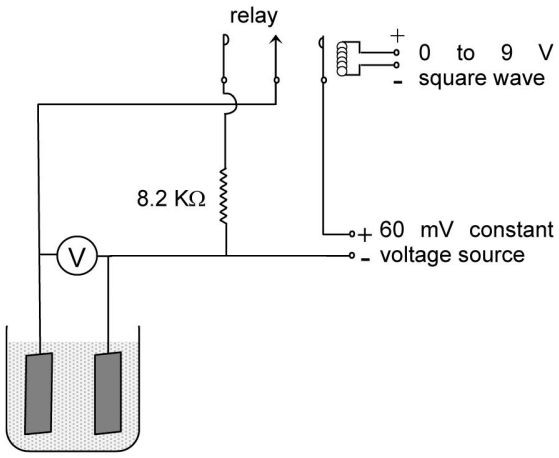
relay
+
0 to 9 V
square wave
8.2 KΩ
+
60 mV constant
voltage source
V

Fig. 1

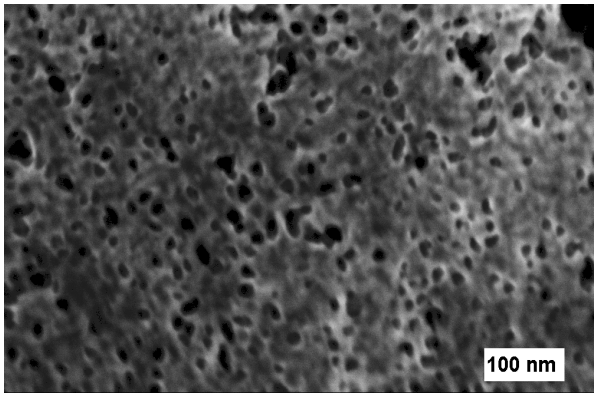

(a)

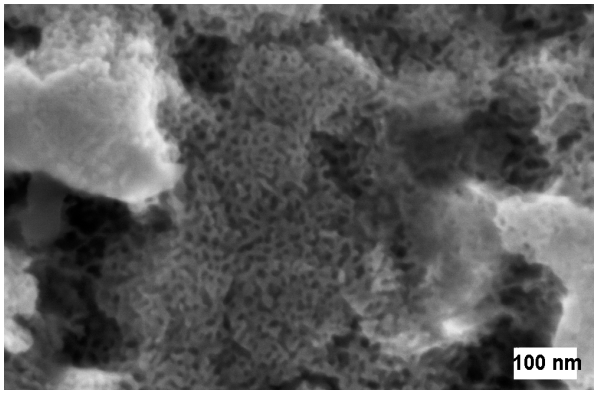

(b)

Fig. 2

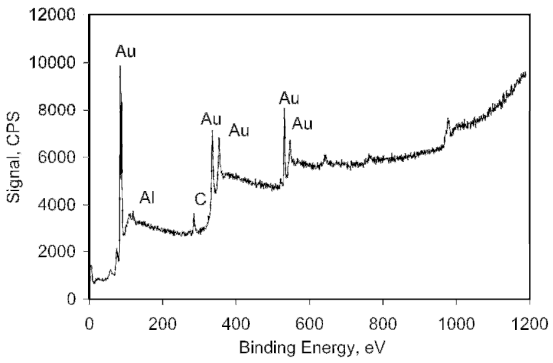
12000
10000
8000
6000
4000
2000
0
Signal, CPS
Au
Al
C
Au
Au
Au
Au
0
200
400
600
800
1000
1200
Binding Energy, eV

(a)

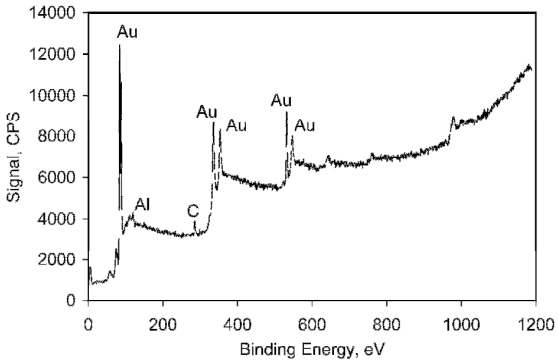
14000
12000
10000
8000
6000
4000
2000
0
Signal, CPS
Au
Al
C
Au
Au
Au
Au
0
200
400
600
800
1000
1200
Binding Energy, eV

(b)

Fig. 3

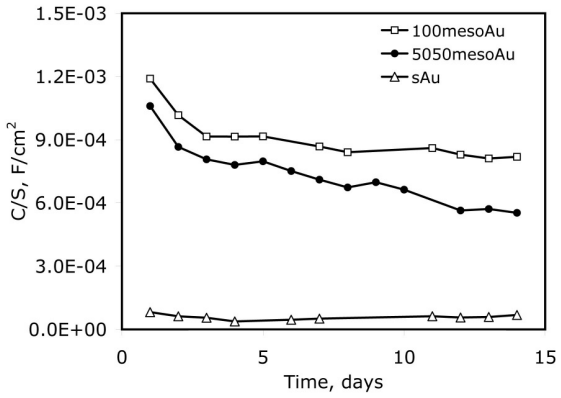
1.5E-03
1.2E-03
9.0E-04
6.0E-04
3.0E-04
0.0E+00
C/S, F/cm2
0
5
10
15
Time, days
100mesoAu
5050mesoAu
sAu

Fig. 4

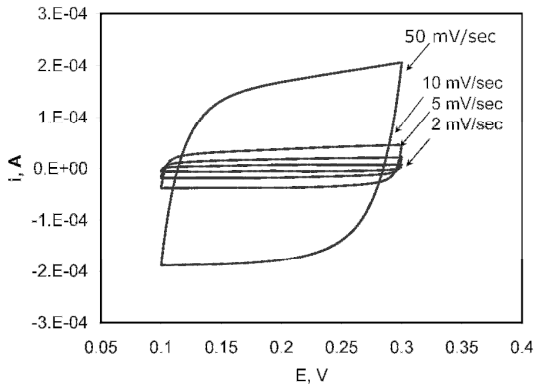
3.E-04
2.E-04
1.E-04
0.E+00
-1.E-04
-2.E-04
-3.E-04
i, A
0.05
0.1
0.15
0.2
0.25
0.3
0.35
0.4
E, V
50 mV/sec
10 mV/sec
5 mV/sec
2 mV/sec

(a)

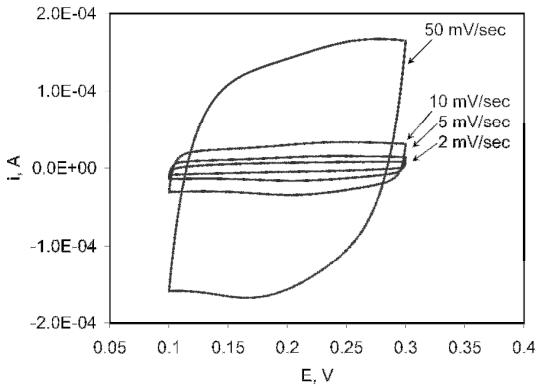
2.0E-04
1.0E-04
0.0E+00
-1.0E-04
-2.0E-04
i, A
0.05
0.1
0.15
0.2
0.25
0.3
0.35
0.4
E, V
50 mV/sec
10 mV/sec
5 mV/sec
2 mV/sec

(b)

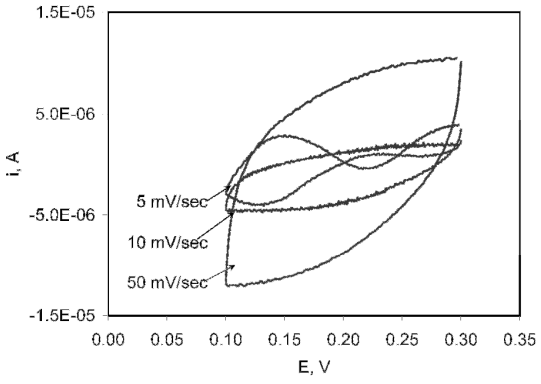
1.5E-05
5.0E-06
-5.0E-06
-1.5E-05
i, A
0.00
0.05
0.10
0.15
0.20
0.25
0.30
0.35
E, V
5 mV/sec
10 mV/sec
50 mV/sec

(c)

Fig. 5

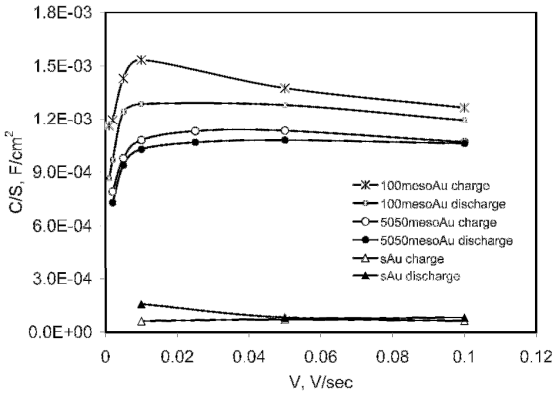
1.8E-03
1.5E-03
1.2E-03
9.0E-04
6.0E-04
3.0E-04
0.0E+00
C/S, F/cm2
0
0.02
0.04
0.06
0.08
0.1
0.12
V, V/sec
100mesoAu charge
100mesoAu discharge
5050mesoAu charge
5050mesoAu discharge
sAu charge
sAu discharge

Fig 6.

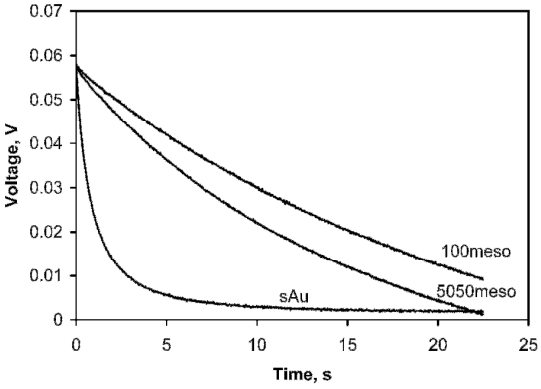
0.07
0.06
0.05
0.04
0.03
0.02
0.01
0
Voltage, V
0
5
10
15
20
25
Time, s
100meso
5050meso
sAu

(a)

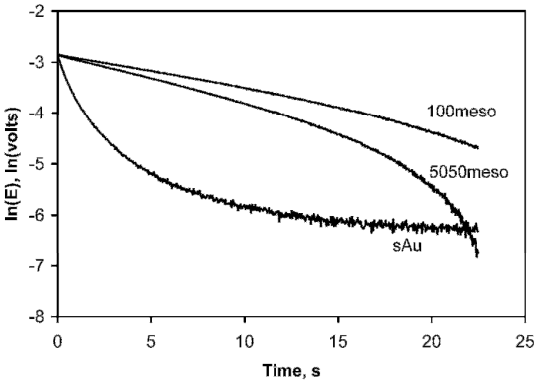
-2
-3
-4
-5
-6
-7
-8
ln(E), ln(volts)
0
5
10
15
20
25
Time, s
100meso
5050meso
sAu

(b)

Fig. 7

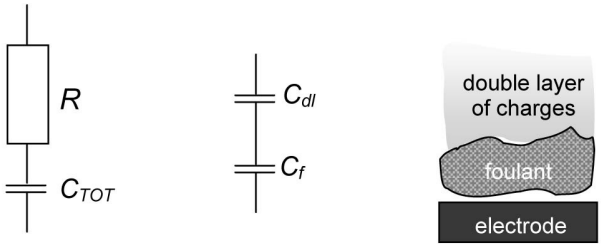

Fig. 8

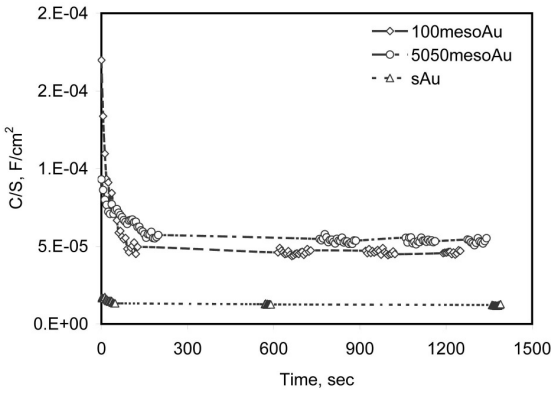
2.E-04
2.E-04
1.E-04
5.E-05
0.E+00
C/S, F/cm2
0
300
600
900
1200
1500
Time, sec
100mesoAu
5050mesoAu
sAu

(a)

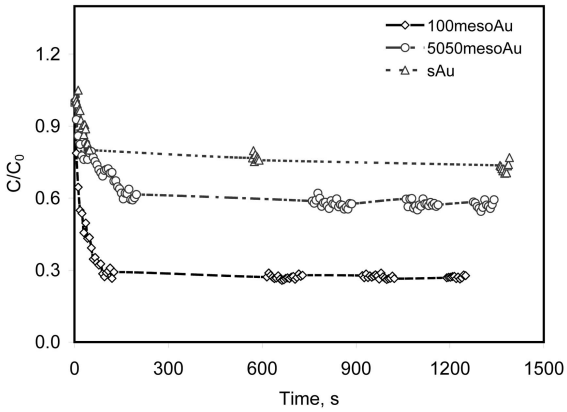
1.2
0.9
0.6
0.3
0.0
C/C0
0
300
600
900
1200
1500
Time, s
100mesoAu
5050mesoAu
sAu

(b)

Fig. 9